Inorg. Chem. **2004**, *43*, 2569–2576

Ionic Pair Complexes with Well-Separated Columnar Stack Structure Based on $[Pt(mnt)_2]^-$ Ions Showing Unusual Magnetic Transition: Syntheses, Crystal Structures, and Magnetic Properties

X. M. Ren,*[,†,‡,§] H. Okudera,[†] R. K. Kremer,[†] Y. Song,[‡] C. He,[∥] Q. J. Meng,[‡] and P. H. Wu[⊥]

Coordination Chemistry Institute & State Key Laboratory and Department of Electronic Science & Engineering, Nanjing University, Nanjing 210093, Department of Chemistry, Anqing Normal College, Anqing 246011, and State Key Lab Of Rare Earth Materials Chemistry & Applications, Peking University, Beijing 100871, People's Republic of China, and Max-Planck-Institut für Festkörperforschung, Heisenbergstrasse 1, Postfach 800665, D-70569 Stuttgart, Germany

Received December 6, 2003

Three ion pair complexes, [4-R-benzylpyridinium][bis(maleodinitriledithiolato)platinum(III)] (abbreviated as [RBzPy]-$[Pt(mnt)_2]$; R = Cl (**1**), Br (**2**), or NO_2 (**3**)), have been synthesized. The cations and anions stack into well-separated columns in the solid state, and the Pt(III) ions form a 1-D zigzag chain within a $[Pt(mnt)_2]^-$ column through Pt···S, S···S, and Pt···S···Pt interactions. The chain is uniform in **1** and **2**, while it alternates in **3**. Unusual magnetic phase transitions from paramagnetism to diamagnetism were observed in these three complexes at ∼275 K for **1**, ∼269 K for **2**, and ∼184 K for **3**. These phase transitions were also found in DSC measurements for **1** and **2**. The overall magnetic behaviors for **1**–**3** indicate the presence of antiferromagnetic exchange interactions in the high-temperature phase and spin-gapped systems in the low-temperature phase. Below 50 K, **2** exhibits weak ferromagnetism. The spontaneous moments are nearly repressed by a field of 1.0 T. The crystal structure of **2** at 173 K reveals that there are two crystallographically independent $[Pt(mnt)_2]^-$ entries in an asymmetric unit. These two crystallographically independent $[Pt(mnt)_2]^-$ entries satisfy the spin-canting condition, and the EPR spectra measured at room temperature exhibit anisotropic character. Therefore, the weak ferromagnetic behavior in the low-temperature region for **2** can be attributed to the spin-canting phenomenon.

Introduction

A lot of research has been devoted to low-dimensional spin systems[1] due to their unusual physical phenomena, such as spin−Peierls transition,[2] charge-density-wave (CDW) states/spin-density-wave (SDW) states,[3] spin−charge separation states,[4] and valence-ordering.[5] In recent years, some new quantum phenomena were found in the quasi-one-dimensional (1-D) spin systems, for instance, slow relaxation of magnetization and hystersis effects which are not associated with 3-D ordering[6a] and distinct plateaus in the magnetization,[6b] which stimulated the investigations in the aspects of both the molecular design and a theory for the low-dimensional spin system.[7]

Our aim is to construct quasi-one-dimensional molecular magnetic materials based on $[M(mnt)_2]^-$ blocks (M = Ni(III),

* Author to correspondence should be addressed. Phone: +49 711 689 1687. Fax: +49 711 689 1689. E-mail: x.ren@fkf.mpg.de.

† Coordination Chemistry Institute & State Key Laboratory, Nanjing University.

‡ Anqing Normal College.

§ Max-Planck-Institut für Festkörperforschung.

∥ Peking University.

⊥ Department of Electronic Science & Engineering, Nanjing University.

(1) Wolf, B.; Zherlitsyn, S.; Schmidt, S.; Lüthi, B. *Phys. Status Solidi A* **2002**, *189*, 389.

(2) (a) Bray, J. W.; Hart, H. R.; Interrante, L. V., Jr.; Jacobs, I. S.; Kasper, J. S.; Watkins, G. D.; Wee, H.; Bonner, J. C. *Phys. Rev. Lett.* **1975**, *35*, 744. (b) Ota, A.; Yamochi, H.; Saito, G. *J. Mater. Chem.* **2002**, *12*, 2600.

(3) (a) Coomber, A. T.; Beljonne, D.; Friend, R. H.; Brédas, J. L.; Charlton, A.; Robertson, N.; Underhill, A. E.; Kurmoo, M.; Day, P. *Nature* **1996**, *380*, 144. (b) Wei, J. H.; Zhao, J. Q.; Liu, D. S.; Xie, S. J.; Mei, L. M.; Hong, J. *Synth. Met.* **2001**, *122*, 305.

(4) Lorenz, T.; Hofmann, M.; Grüninger, M.; Freimuth, A.; Uhrig, G. S.; Dumm, M.; Dressel, M. *Nature* **2002**, *418*, 614.

(5) Mitsumi, M.; Kitamura, K.; Morinaga, A.; Ozawa, Y.; Kobayashi, M. *Angew. Chem., Int. Ed.* **2002**, *41*, 2767.

(6) (a) Caneschi, A.; Gatteschi, D.; Lalioti, N.; Sangregorio, C.; Sessoli, R.; Venturi, G.; Vindigni, A.; Rettori, A.; Pini, M. G.; Novak, M. A. *Angew. Chem., Int. Ed.* **2001**, *40*, 1760. (b) Shiramura, W.; Takatsu, K.; Kurniawan, B.; Tanaka, H.; Uekusa, H.; Ohashi, Y.; Takizawa, K.; Mitamura, H.; Goto, T. *J. Phys. Soc. Jpn.* **1998**, *67*, 1548.

10.1021/ic035405+ CCC: $27.50 © 2004 American Chemical Society
Published on Web 03/25/2004

Chart 1

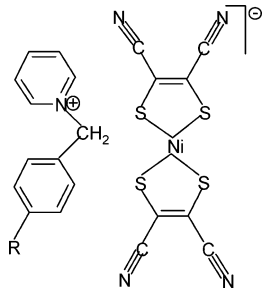

Pd(III), and Pt(III); mnt^{2-} = maleodinitriledithiolate), which have been intensively studied in molecular conductors and magnets.[8−11] More recently, we have developed a new class of salts, $[RBzPy]^+[Ni(mnt)_2]^-$, where $[RBzPy]^+$ denotes the benzylpyridinium derivatives (refer to Chart 1). In these ionic pair compounds, the prominent structural feature is that the anions and cations stack into completely segregated columns; the Ni(III) ions within an anionic column hence form a quasi-one-dimensionally spaced magnetic chain through intermolecular S···S, Ni···Ni, S···Ni, or $\pi-\pi$ interactions.[12] Another significant finding is that a lot of compounds exhibit an unusual magnetic phase transition from paramagnetism to diamagnetism.[12a−d] To extend our research and understand these novel magnetic properties, we further pursue the study of $[RBzPy]^+[Pt(mnt)_2]^-$ because the $[Pt(mnt)_2]^-$ anion is similar to the $[Ni(mnt)_2]^-$ anion in both the molecular and electronic structures. In this paper, we report the syntheses, crystal structures, and magnetic properties of three $[Pt(mnt)_2]^-$ complexes.

Results and Discussion

Crystal Structure of 1 at 293 K. Figure 1 shows the ORTEP drawing of **1**. The Pt(III) ion in the $[Pt(mnt)_2]^-$ moiety is coordinated by four S atoms of two mnt^{2-} ligands, and exhibits square-planar coordination geometry. The CN groups of the mnt^{2-} ligand are out of the coordinating plane defined by the four S atoms; the deviations of N atoms from the coordinated plane are 0.17 Å for N(1), 0.26 Å for N(2), 0.43 Å for N(3), and 0.27 Å for N(4). The average S−Pt−S bond angle in the chelating ring is 89.8°, and the average Pt−S bond distance is 2.26 Å. These values are in closed agreement with the results reported for other $[Pt(mnt)_2]^-$ complexes.[9,13] In the $[ClBzPy]^+$ moiety, the benzene ring/pyridine ring with the reference plane C(15)/C(14)/N(5) makes a dihedral angle of 98.1°/84.0°, respectively. The aromatic rings are approximately perpendicular to the reference plane. This result can be compared with that reported for $[ClBzPy][Ni(mnt)_2]$.[12a]

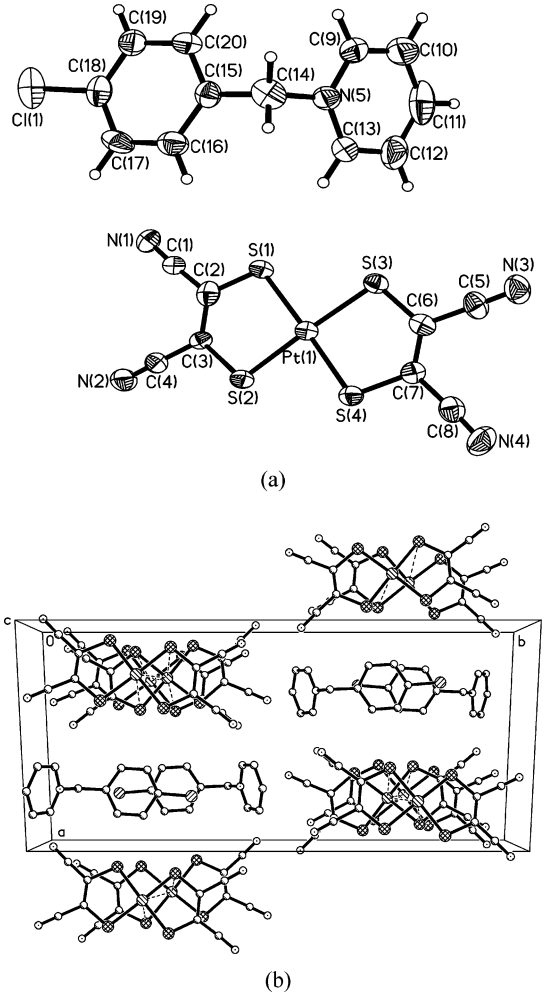

Figure 1. (a) ORTEP view of **1** with 30% probability thermal ellipsoids. (b) Completely separated columnar stacking of **1** along the *c*-axis.

The anions and cations stack into well-separated columns along the crystallographic *c*-axis (Figure 1b). In an anionic column, two adjacent $[Pt(mnt)_2]^-$ anions slide along the bisector direction of the bonding angle S−Pt−S of the chelating ring, and overlap as displayed in Figure 2; the interplane (coordinated planes) distances between adjacent anions are 3.66 and 3.60 Å. The adjacent Pt(III) ions have equal separations (the Pt···Pt distance is 3.88 Å, beyond metal−metal bonding distance[9]). The nearest S···S and S···Pt contacts have distances of 3.71 and 3.77 Å, respec-

(7) (a) Oshikawa, M.; Yamanaka, M.; Affleck, I. *Phys. Rev. Lett.* **1997**, *78*, 1984. (b) Totsuka, K. *Phys. Rev. B* **1998**, *57*, 3454.

(8) Nishijo, J.; Ogura, E.; Yamaura, J.; Miyazaki, A.; Enoki, T.; Takano, T.; Kuwatani, Y.; Iyoda, M. *Solid State Commun.* **2000**, *116*, 661.

(9) Pullen, A. E.; Faulmann, C.; Pokhodnya, K. I.; Cassoux, P.; Tokumoto, M. *Inorg. Chem.* **1998**, *37*, 6714.

(10) Allan, M. L.; Coomber, A. T.; Marsden, I. R.; Martens, J. H. F.; Friend, R. H.; Charlton, A.; Underhill A. E. *Synth. Met.* **1993**, *55*−*57*, 3317.

(11) Kobayashi, A.; Sasaki, Y.; Kobayashi, H.; Underhill, A. E.; Ahmad, M. M. *J. Chem. Soc., Chem. Commun.* **1982**, 390.

(12) (a) Ren, X. M.; Meng, Q. J.; Song, Y.; Hu, C. J.; Lu, C. S.; Chen, X. Y. *Inorg. Chem.* **2002**, *41*, 5686. (b) Xie, J. L.; Ren, X. M.; Song, Y.; Zhang, W. W.; Liu, W. L.; He, C.; Meng, Q. J. *Chem. Commun.* **2002**, 2346. (c) Xie, J. L.; Ren, X. M.; He, C.; Gao, Z. M.; Song, Y.; Meng, Q. J.; Kremer, R. K. *Chem. Phys. Lett.* **2003**, *369*, 41. (d) Ren, X. M.; Meng, Q. J.; Song, Y.; Lu, C. S.; Hu, C. J.; Chen, X. Y.; Xue, Z. L. *Inorg. Chem.* **2002**, *41*, 5931. (e) Xie, J. L.; Ren, X. M.; Song, Y.; Tong, W. J.; Lu, C. S.; Yao, Y. G.; Meng, Q. J. *Inorg. Chem. Commun.* **2002**, *5*, 395. (f) Xie, J. L.; Ren, X. M.; Song, Y.; Zou, Y.; Meng, Q. J. *J. Chem. Soc., Dalton Trans.* **2002**, 2868. (g) Xie, J. L.; Ren, X. M.; Gao, S.; Zhang, W. W.; Li, Y. Z.; Lu, C. S.; Ni, C. L.; Liu, W. L.; Meng, Q. J.; Yao, Y. G. *Eur. J. Inorg. Chem.* **2003**, 2393. (h) Ren, X. M.; Lu, C. S.; Liu, Y. J.; Zhu, H. Z.; Li, H. F.; Hu, C. J.; Meng, Q. J. *Transition Met. Chem. (Dordrecht, Neth.)* **2001**, *26*, 136.

(13) (a) Kobayashi, A.; Sasaki, Y.; Kobayashi, H.; Underhill, A. E.; Ahmad, M. M. *Chem. lett.* **1984**, 305. (b) Kobayashi, A.; Sasaki, Y.; Kobayashi, H.; Underhill, A. E.; Ahmad, M. M. *Chem. Commun.* **1982**, 390. (c) Bois, H.; Connelly, N. G.; Crossley, J. G.; Guillorit, J.-C.; Lewis, G. R.; Orpen, A. G.; Thornton, P. *J. Chem. Soc., Dalton Trans.* **1998**, 2833.

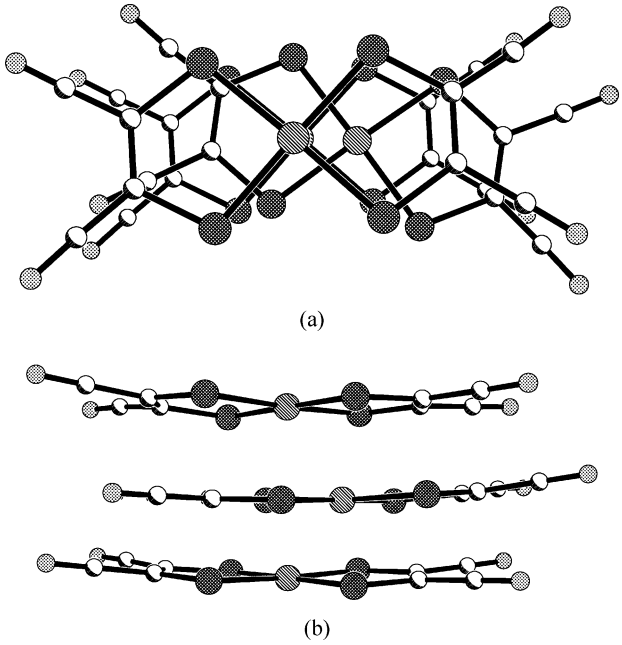

Figure 2. Overlapping pattern of [Pt(mnt)$_2$]$^-$ anions in **1**: (a) top view; (b) side view.

tively. Within a column of [ClBzPy]$^+$, the adjacent cations stack into a boat-type conformation (Figure 3a), which is same as that for the Ni(III)-based complexes. The center-to-center distances between the face-to-face stacking of benzene rings are the same (4.17 Å), and too long to be of energetic significance for $\pi\cdots\pi$ stacking interaction.[14] There are only weak van de Waals interactions between the adjacent cationic and anionic columns. The closest Pt$\cdots$Pt separation between anionic columns is 12.22 Å, which is significantly longer than the Pt$\cdots$Pt distance in a column, so **1** should be an ideal 1-D spin system with $S = 1/2$ from the viewpoint of the structure.

Crystal Structures of 2 and 3 at 293 K. Complexes **2** and **3** were isostructural with **1** at room temperature; the bond parameters in the anionic [Pt(mnt)$_2$]$^-$ entries are compared with the values for **1** and presented in Table 1. The nearest-neighbor interplane distances in an anionic column are 3.61/3.64 Å for **2** and 3.44/3.56 Å for **3** (Table 2). The Pt$\cdots$Pt separations between nearest neighbors in an anionic column are identical (3.90 Å) for **2**, and alternate as 3.46/4.08 Å for **3**. Hence, the chain formed by Pt(III) ions in an anionic column is uniform in **2**, while it dimerize in **3**. The adjacent cations stack into a column via the boat-type conformation in **2**, and the chair-type conformation in **3** (Figure 3b), while the cations stack into a column by the boat-type conformation in the corresponding Ni(III)-based complexes.[12a] The center-to-center distances between face-to-face benzene rings are 4.30 Å for **2** and 4.05/4.55 Å for **3**.

By comparing the structures of **1**−**3** with the corresponding Ni(III)-based complexes, we conclude that the complexes consisting of planar [M(mnt)$_2$]$^-$ and the derivatives of benzylpyridinium with a Λ-shaped molecular configuration favor columnar molecular stacking.

(14) Vangala, V. R.; Nangia, A.; Lynch, V. M. *Chem. Commun.* **2002**, 1304.

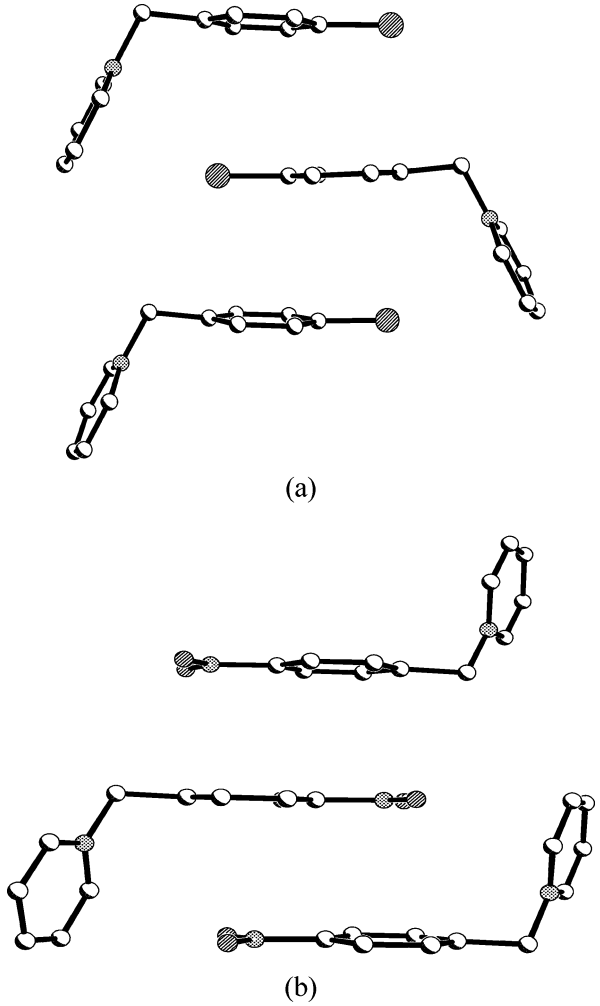

Figure 3. Stacking patterns of the cations: (a) boat-type conformation in **1**; (b) chair-type configuration in **3** (H atoms omitted for clarity).

Table 1. Selected Bond Parameters in [Pt(mnt)$_2$]$^-$ Anionic Moieties for **1**−**3**

	1	**2** (293 K)	**2** (173 K)	**3**
		Bond Lengths (Å)		
Pt1−S1	2.255(3)	2.2656(16)	2.271(2)	2.2571(14)
Pt1−S2	2.260(3)	2.2578(16)	2.263(2)	2.2677(15)
Pt1−S3	2.266(3)	2.2718(17)	2.254(2)	2.2541(15)
Pt1−S4	2.249(3)	2.2536(17)	2.275(2)	2.2656(14)
Pt2−S5			2.253(2)	
Pt2−S6			2.271(2)	
Pt2−S7			2.258(2)	
Pt2−S8			2.267(2)	
		Bond Angles (deg)		
S1−Pt1−S2	89.80(10)	89.55(6)	90.06(7)	89.87(5)
S1−Pt1−S3	91.81(11)	91.94(6)	88.84(7)	88.23(6)
S1−Pt1−S4	178.25(11)	178.24(6)	175.66(8)	177.94(5)
S2−Pt1−S3	176.54(10)	176.04(7)	178.64(7)	177.69(5)
S2−Pt1−S4	88.54(11)	88.71(6)	91.18(7)	92.14(5)
S3−Pt1−S4	89.88(11)	89.81(6)	89.97(7)	89.77(6)
S5−Pt2−S6			89.95(7)	
S5−Pt2−S7			88.13(7)	
S5−Pt2−S8			178.10(7)	
S6−Pt2−S7			176.41(8)	
S6−Pt2−S8			91.85(7)	
S7−Pt2−S8			90.04(7)	

Magnetic Properties of 1−3. Temperature dependence studies of magnetic susceptibility for **1**−**3** were carried out on polycrystalline samples at the external field of 0.1 T; the

Table 2. Intermolecular Shorter Separations between Nearest-Neighbor Anions (Å) for **1**−**3** at 293 K

	1		**2**		**3**	
overlap	AB	BA′	AB	BA′	AB	BA′
Pt···Pt	3.8845(9)	3.8845(9)	3.8965(7)	3.8965(7)	3.4558(8)	4.0843(9)
Pt···S	Pt(1)···S(2) 3.7676(29)	Pt(1)···S(1) 3.8144(30)	Pt(1)···S(1) 3.7838(20)	Pt(1)···S(1) 3.7943(19)	Pt(1)···S(4) 3.9360(17)	Pt(1)···S(4) 3.7871(18)
S···S	S(2)···S(4) 3.7041(44)	S(2)···S(4) 3.8837(45)	S(2)···S(4) 3.7045(28)	S(2)···S(4) 3.9207(28)	S(1)···S(4) 3.4319(21) S(2)···S(3) 3.5155(22)	S(2)···S(3) 3.7885(22)
	Symmetry Operation Applied on the Second Atom for AB or BA′					
	x, 1.5 − y, −0.5 + z	x, 1.5 − y, 0.5 + z	x, 1.5 − y, −0.5 + z	x, 1.5 − y, 0.5 + z	−x, 2 − y, −z	1 − x, 2 − y, −z

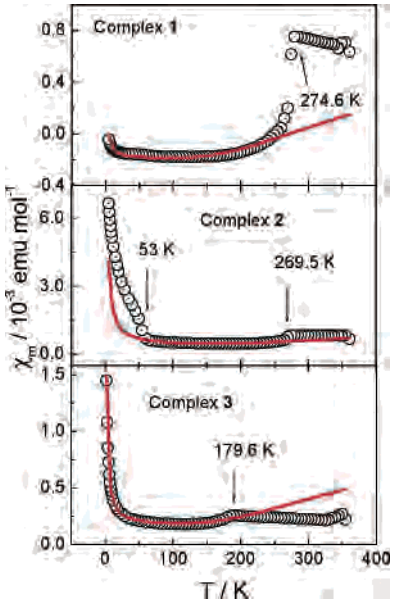

Figure 4. Temperature dependence of the magnetic susceptibility for **1**−**3**. Open circles represent experimental data, and the solid lines are reproduced from the theoretic calculations and detailed fitting procedure described in the text.

plots of χ_m versus T are illustrated in Figure 4. The magnetic susceptibility abruptly drops as temperature decreases for **1**−**3**. On increasing the temperature back to the original one, the plots of χ_m−T were almost identical, and no sizable hysteresis effects were detected. This finding indicates these three complexes undergo a reversible phase transition. The phase transition temperature is evaluated as the temperature at the maximum of the d($\chi_m T$)/dT derivative, namely, ∼274.6 K is for **1**, ∼269.5 K for **2**, and ∼179.6 K for **3**.

In the high-temperature phase (HT phase), the overall magnetic behaviors of **1**−**3** correspond to a paramagnetic system with an antiferromagnetic coupling interaction. As the temperature decreases, the values of $\chi_m T$ slightly decrease from 0.230 emu K mol^{-1} at 360 K to 0.210 emu K mol^{-1} at 279 K for **1** (the values of $\chi_m T$ are more less than that for an isolated magnetic system with $S = 1/2$; this means there are short-range magnetic correlations between neighbor spins), decrease from 0.238 emu K mol^{-1} at 360 K to 0.231 emu K mol^{-1} at 274 K for **2**, and strongly decrease from 0.785 emu K mol^{-1} at 360 K to 0.388 emu K mol^{-1} at 175 K for **3**. In the low-temperature phase (LT phase), the magnetic susceptibilities of **1**−**3** decrease exponentially as the sample temperature decreases, and exhibit the characteristics of a spin gap system. In comparison of the magnetic behaviors among **1**−**3**, **2** is different from **1** and **3**. The plots of the magnetic susceptibility of both **1** and **3** exist as Curie tails, which arise from uncoupled magnetic impurities; however, the magnetic susceptibility of **2** increases sharply below ∼50 K to distinctly show a weakly ferromagnetic ordering feature, which will be discussed further in detail in a later section.

For a spin gap system, the magnetic susceptibility may be estimated by the formula $\chi_m = [\alpha \exp(-\Delta/k_B T)]/T + C/T + \chi_0$, where α is a constant value corresponding to the dispersion of excitation energy, Δ is the magnitude of the spin gap, χ_0 contributes from the core diamagnetism and the possible Van Vleck paramagnetism, and the other symbols have their usual meaning.[15] The best fit curves for **1**−**3** are shown in Figure 4, and the corresponding parameters are given as follows: $\alpha = 1.72$, $\Delta/k_B = 948.1$ K, $\chi_0 = -2.3 \times 10^{-4}$ emu mol^{-1}, $C = 9.4 \times 10^{-4}$ emu K mol^{-1} obtained from the data in the temperature range 5−245 K (assuming the magnetic impurity arises from uncoupled Pt(III) ions with $S = 1/2$ and the g factor is near 2.0, the concentration of the magnetic impurity is estimated as ∼0.2%), and agreement factor $R = 4.1 \times 10^{-3}$ [R is defined as $\sum_i(\chi_m^{calcd} - \chi_m^{obsd})^2/(\chi_m^{obsd})^2$] for **1**. $\alpha = 1.92$, $\Delta/k_B = 998.0$ K, $\chi_0 = 3.3 \times 10^{-4}$ emu mol^{-1}, $C = 1.8 \times 10^{-3}$ emu K mol^{-1} on the basis of the data in the temperature range 59−252 K (the corresponding content of the magnetic impurity is ∼0.5%), and agreement factor $R = 1.4 \times 10^{-3}$ for **2**. $\alpha = 1.64$, $\Delta/k_B = 942.8$ K, $\chi_0 = 1.6 \times 10^{-4}$ emu mol^{-1}, $C = 3.0 \times 10^{-3}$ emu K mol^{-1} from the magnetic susceptibility data in the temperature range 2−165 K (the corresponding content of the magnetic impurity is ∼0.8%), and agreement factor $R = 1.1 \times 10^{-3}$ for **3**. On the basis of the above results, the values of the parameter $2\Delta/k_B T_C$ (T_C is the transition temperature) are estimated to be 6.9, 7.4, and 10.5 for **1**−**3**, respectively. These values are higher than the ideal value of 3.53 derived from the BCS formula in a weak coupling regime. These results thus mean that the short-range magnetic correlations within a chain are not fully developed and intrinsic magnetoelastic instability of a 1-D system cannot be considered as a driving force for this transition; namely, the transition is not a pure spin−Peierls transition. [12a]

Crystal Structure of 2 at 173 K (LT Phase). To clarify the structural changes of these compounds, we determined the crystal structure of **2** at 173 K, well below the phase transition temperature. Comparing the crystallographic parameters at 173 K with those at room temperature, it is found

(15) Isett, L. C.; Rosso, D. M.; Bottger, G. L. *Phys. Rev. B* **1980**, *22*, 4739.

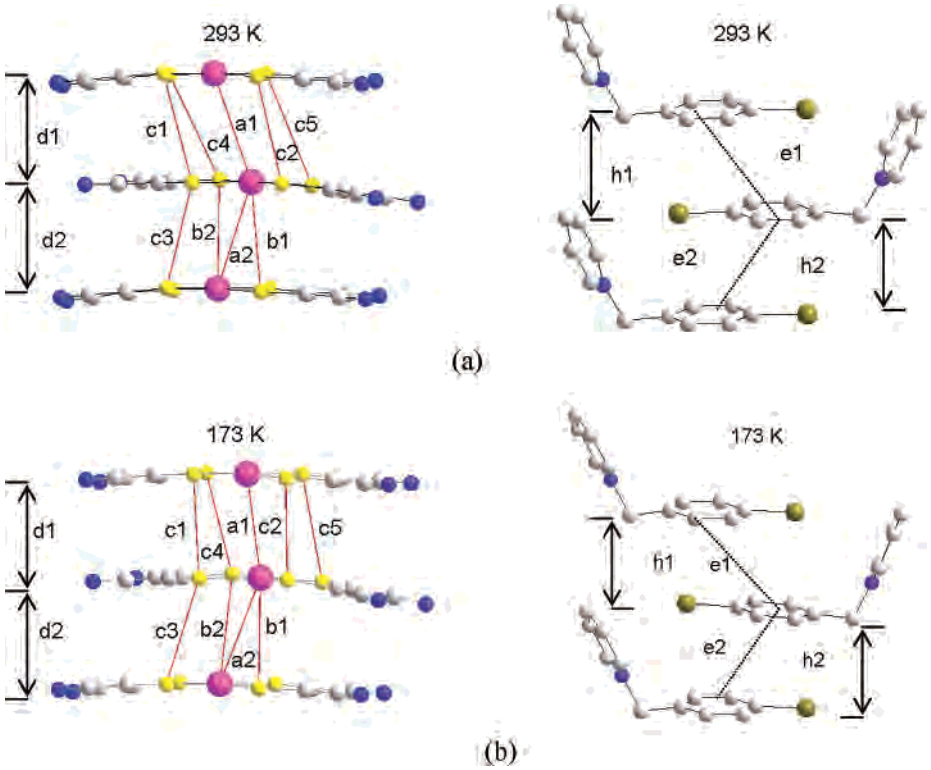

Figure 5. Scheme indicating the separations of both interatoms and intermolecular planes. a1, a2, b1, b2, c1−c5, d1, d2, e1, e2, h1, and h2 represent the Pt···Pt, Pt···S, S···S, anionic plane-to-plane (defined by four coordinated S atoms), and benzene ring center-to-center and plane-to-plane separations.

that this compound crystallizes in space group $P2(1)/c$ at room temperature (HT phase) but $P\bar{1}$ at low temperature (LT phase). In an asymmetric unit, one couple of 4-brominobenzylpyridinum and $[Pt(mnt)_2]^-$ in the HT phase changes into two couples of ionic pairs in the LT phase. The molecular structures in the LT and HT phases are almost identical, as illustrated in Figure 5. The Pt(III) ions are still positioned in a zigzag fashion in an anionic column, but the nearest-neighbor distances of Pt···Pt within an anionic column alternate as 3.96 Å (almost unchanged compared with the result of 3.90 Å in the HT phase) and 3.55 Å (decreasing by ∼9%). In an anionic column, the plane-to-plane separations between the neighbor anions are 3.66 and 3.45 Å. The former value is comparable with the result in the HT phase, but the latter decreases by ∼3%. Other distances of atomic pairs (Pt···S and S···S) in both intra- and interstacks are summarized in Table 3. Obviously, this phase transition occurs along with the dimerization of the adjacent anions.

Thermodynamic Properties of the Phase Transition for 1−3. The power-compensated DSC traces for **1** and **2** from 223 to 283 K at a warming rate of 20 K min^{-1} are displayed in Figure 6. Clearly, **1** and **2** exhibit similar thermodynamic behavior; abruptly endothermic peaks in their DSC traces are observed. The phase transition temperatures determined from thermal analyses are 274.3 K for **1** and 268.9 K for **2**, close to their values measured from magnetic susceptibility measurements. The endothermic enthalpy changes (ΔH), which were estimated from the peak areas, are 452.9 J mol^{-1} for **1** and 59.7 J mol^{-1} for **2** (the enthalpy of the phase transition of **1** is greater than that of **2**). Therefore, the results of thermal analyses of **1** and **2** further confirm that the phase

Table 3. Geometric Parameters (Å) between Intra- and Interstacks of Both the Anion and Cation for **2**

		293 K	173 K
Pt···Pt	a1	3.8965(7)	3.5458(9)
	a2	3.8965(7)	3.9605(10)
Pt···S	b1	3.7943(19)	3.8119(25)
	b2	3.7838(20)	3.8418(24)
S···S	c1	3.9207(28)	3.5948(31)
	c2	3.7045(28)	3.4259(31)
	c3	3.7045(28)	3.7839(30)
	c4	4.0018(27)	3.5840(31)
	c5	4.0751(28)	3.6948(32)
plane-to-plane (coordinated plane)	d1	3.6419(30)	3.44803(34)
	d2	3.6140(30)	3.6576(36)
center-to-center (benzene ring)	e1	4.30	4.08
	e2	4.30	4.51
plane-to-plane (benzene ring)	h1	3.6094(91)	3.5250(127)
	h2	3.6191(87)	3.6709(140)

transitions observed are first-order.[16] In contrast to **1** and **2**, the DSC measurement of **3** showed no observable endothermic peak in the corresponding temperature region around the magnetic phase transition (Figure 6b).

We deduced that the entropy difference of the phase transition is about 1.65 J mol^{-1} K for **1** and 0.22 J mol^{-1} K for **2** according to $\Delta S = \Delta H/T_C$ and the enthalpies estimated above. The magnetic entropy can be calculated according to $\Delta S = R \ln[(2S_{HT} + 1)/(2S_{LT} + 1)] = R \ln 2 \approx 5.76$ J mol^{-1} K, where $R = 8.31441$ J mol^{-1} K is the gas constant.[17] The estimated entropy change from DSC experiments is

(16) (a) Hatta, I.; Nakayama, S. *Thermochim. Acta* **1998**, *318*, 21. (b) Jakubas, R.; Clapala, P.; Pietraszko, A.; Zaleski, J.; Kusz, J. *J. Phys. Chem. Solids* **1998**, *59*, 1309. (c) Tang, T.; Gu, K. M.; Cao, Q. Q.; Wang, D. H.; Zhang, S. Y.; Du Y. W. *J. Magn. Magn. Mater.* **2000**, *222*, 110.

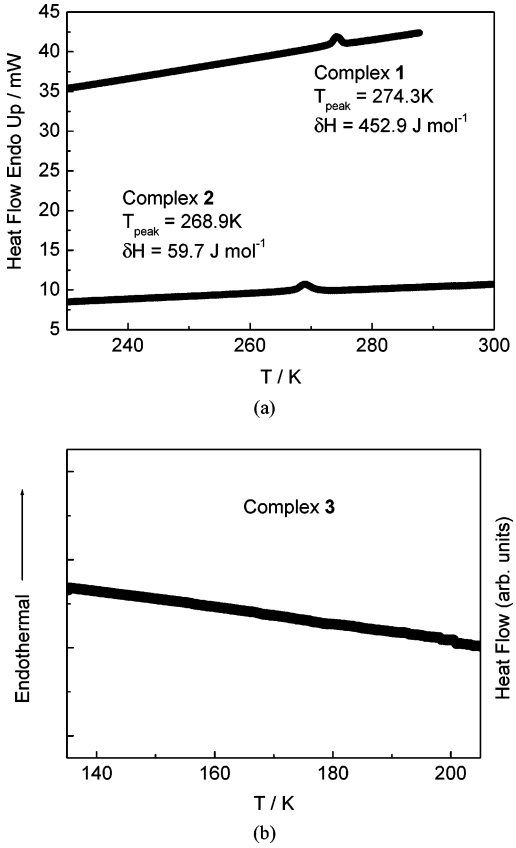

Figure 6. DSC plots (a) for **1** and **2** and (b) for **3**.

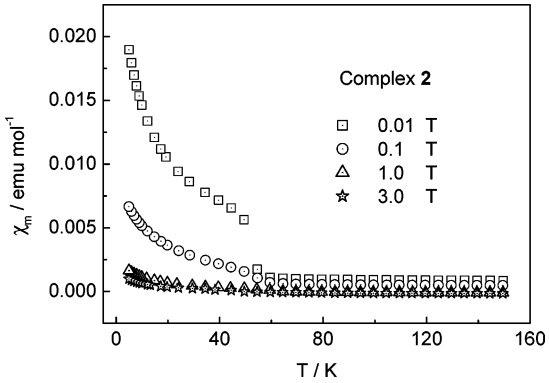

Figure 7. Field-cooled magnetic susceptibility for **2** under different magnetic fields.

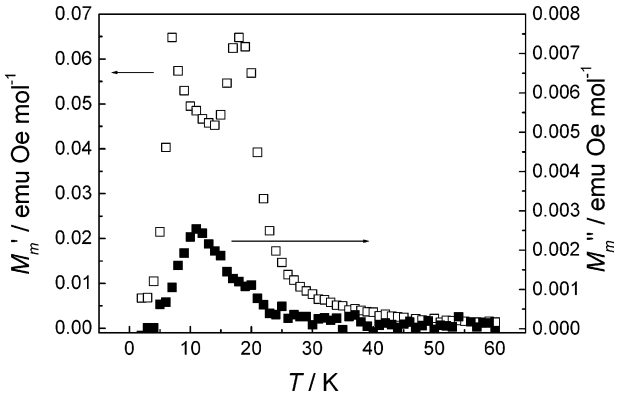

Figure 8. ac magnetizations of zero field for **2** at a frequency of 115 Hz.

equal to the magnetic entropy alone of ~29% for **1** and ~4% for **2**. The entropy changes for **1** and **2** are much less than 5.76 J mol^{-1} K, which is expected from the short-range order effects between nearest-neighbor spins in the HT phase,[19b] and this is in agreement with the effective magnetic moments of **1** and **2** in the HT phase being much less than the calculated value for an isolated magnetic system with $S = 1/2$.

Weak Ferromagnetic Behavior of 2 below 50 K. Field-cooled magnetization measurements were performed under 0.01, 0.1, 1.0, and 3.0 T (Figure 7). Under these fields, **2** exhibits weak ferromagnetic character as indicated by the χ_m values abruptly increasing below ~50 K, the magnetic transitions are less pronounced at higher fields, and the spontaneous moments are nearly repressed by a field of 1.0 T. The ferromagnetic properties are further illustrated by ac susceptibility measurements with zero magnetic field at a frequency of 115 Hz. Typically, for a magnet with net magnetic moments in the ordered state (for instance, ferromagnet, ferrimagnet, or canted antiferromagnet), a maximum in the in-phase signal (χ') is near T_C and the out-of-phase signal (χ'') starts to appear at temperatures just below T_C. Figure 8 shows the maximum of χ' at around 18 K and the corresponding peak of χ'' at around 11 K. These results reveal the weak ferromagnetic ordering below ~18 K. Another maximum in the in-phase signal at ~7 K indicates another magnetic phase transition; perhaps this complicated magnetic behavior is similar to that in some alloy systems, that is, reentrant spin glass behavior.[18] However, the nature of this phase transition is unclear, and its investigation is in progress.

The isothermal magnetizations were measured at 5, 10, and 50 K (Figure 9). The maximum value of the magnetization at 5 K is much smaller than the theoretical saturation value of an $S = 1/2$ with $g = 2.0$ system.

The maximum magnetization reaches only 2.2 emu Oe mol^{-1} at 5 K; this magnetization is significantly lower than the value anticipated for a purely ferromagnetic material of $S_{Pt} = 1/2$, and is contributed as a consequence of spin-canted antiferromagnetism. Spin canting arises through a Dzyaloshinsky−Moriya interaction,[19] and is described by the following Hamiltonian:

$$H_{DM} = -2\sum_{\langle i,j\rangle} \mathbf{d}(S_i \cdot S_j)$$

This kind of anisotropic exchange interaction involves a combination of spin−orbital coupling and exchange interaction when certain particular symmetry conditions are

(17) Vilminot, S.; Richard-Plouet, M.; André, G.; Swierczynski, D.; Bourée, F.; Kurmoo, M. *Inorg. Chem.* **2003**, *42*, 6859.
(18) (a) Dho, J.; Kim, W. S.; Hur, N. H. *Phys. Rev. Lett.* **2002**, *89*, 27202. (b) Takeuchi, J.; Ishikawa, G.; Miyoshi, K.; Fujiwara, K. *Physica B* **2000**, *284*−*288*, 1165.
(19) (a) Kahn, O. *Molecular Magnetism*; VCH: New York, 1993. (b) Carlin, R. L. *Magnetochemistry*; Springer: Berlin, 1989. (c) Banister, A. J.; Bricklebank, N.; Lavender, I.; Rawson, J. M.; Gregory, C. I.; Tanner, B. K.; Clegg, W.; Elsegood, M. R. J.; Palacio, F. *Anngew. Chem., Int. Ed. Engl.* **1996**, *35*, 2533. (d) Palacio, F.; Antorrena, G.; Castro, M.; Burriel, R.; Rawson, J.; Simith, J. N. B.; Bricklebank, N.; Novoa, J.; Ritter, C. *Phys. Rev. Lett.* **1997**, *79*, 2336. (e) Robertson, N.; Bergemann, C.; Becker, H.; Agarwal, P.; Julian, S. R.; Friend, R. H.; Hatton, N. J.; Underhill, A. E.; Kobayashi, A. *J. Mater. Chem.* **1999**, *9*, 1713.

Table 4. Crystallographic Data for **1**−**3**

	1 (293 K)	**2** (293 K)	**2** (173)	**3** (293)
empirical formula	$C_{20}H_{11}ClN_5PtS_4$	$C_{20}H_{11}BrN_5PtS_4$	$C_{20}H_{11}BrN_5PtS_4$	$C_{20}H_{11}N_6O_2PtS_4$
CCDC no.	CCDC 187749	CCDC 187748		CCDC 187750
mol wt	680.12	724.58	724.58	690.68
space group	$P2_1/c$	$P2_1/c$	$P\bar{1}$	$P2_1/n$
a/Å	12.220(3)	12.181(2)	7.2682(15)	7.1670(14)
b/Å	26.555(6)	26.728(5)	12.249(2)	26.388(5)
c/Å	7.3450(17)	7.4012(15)	26.612(5)	12.624(3)
α/deg	90	90	87.55(3)	90
β/deg	103.734(4)	103.71(3)	84.86(3)	105.65(3)
γ/deg	90	90	75.52(3)	90
V/Å^3	2315.3(9)	2340.9(8)	2284.1(8)	2299.0(8)
Z	4	4	4	4
μ/mm^{-1}	6.555	8.076	8.277	6.498
λ/Å	0.71073	0.71073	0.71073	0.71073
ρ/g cm^{-1}	1.951	2.056	2.107	1.995
R1[a]	0.0657	0.0336	0.0385	0.0407
wR2[a]	0.1312	0.0349	0.0961	0.0455

[a] $R1 = \sum(||F_o| - |F_c||)/\sum|F_o|$; $wR2 = \sum w(|F_o|^2 - |F_c|^2)^2/\sum w(|F_o|^2)^2]^{1/2}$.

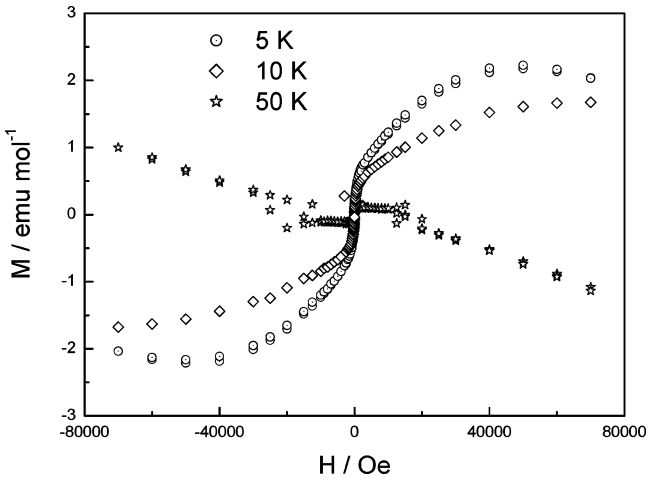

Figure 9. M versus H for **2** at 5, 10, and 50 K.

present. In the low-temperature phase of **2**, two crystallographically independent anions of [Pt(mnt)$_2$]$^-$ with $S = 1/2$ in an asymmetric unit satisfy these conditions. The order of magnitude of the Dzyaloshinsky−Moriya vector **d** can be estimated using the relation $|\mathbf{d}/J| = (g - g_e)/g$.[19] The EPR spectrum of a polycrystalline sample measured at room temperature for **2** showed the anisotropic characterization as shown in the Supporting Information.

Conclusion and Remarks

The crystal structures of three [Pt(mnt)$_2$]$^-$-based complexes at room temperature illustrate that the anions and cations possess well-separated stacking columns as do the series of [Ni(mnt)$_2$]$^-$-based complexes. The column of the [Pt(mnt)$_2$]$^-$ anions is uniform in **1** and **2**, but dimerizes in **3**; however, the anionic column in all [Ni(mnt)$_2$]$^-$-based complexes is uniform. These findings indicate the anionic property effects on the stacking structure of this type of complexes also except for the cationic size and topology. The measurements of the temperature dependence of the magnetic susceptibility reveal the three complexes undergo the magnetic phase transition from paramagnetism to diamagnetism. The phase transitions were observed in the DSC determinations for **1** and **2** also, but not for **3**. The phase transition from paramagnetism to diamagnetism for **1** and **2** is first-order, and the phase transitions with first-order characteristics were verified by crystal structure analysis in the LT phase for **2**. The origins of the phase transitions are attributed to cooperative interactions, such as $\pi-\pi$ stacking interactions between the adjacent cations, Pt···S bonding, interplane repulsion of the [Pt(mnt)$_2$]$^-$ anion,[20] spin−spin coupled interaction between nearest-neighbor anions,[21] and electron(spin)−lattice interactions.[22] In the low-temperature regions, complex **2** exhibits weak ferromagnetism, which should result from the spin-canting phenomenon. The weak ferromagnetism was nearly repressed by a field up to 1.0 T; this phenomenon was observed in some other magnetic systems.[23]

Experimental Section

Materials. Disodium maleonitriledithiolate (Na_2mnt) and 1-(4′-R-benzyl)pyridinium chloride ([RBzPy]Cl) were prepared by the literature procedures,[24,25] where R = Cl, Br, and NO_2, respectively. [RBzPy]$_2$[Pt(mnt)$_2$] were prepared by a similar method described in the literature. [25]

Preparations of the Complexes. [ClbzPy][Pt(mnt)$_2$] (1). A MeCN solution (10 mL) of I_2 (150 mg, 0.59 mmol) was slowly added to a MeCN solution (20 mL) of [ClbzPy]$_2$[Pt(mnt)$_2$] (813 mg, 1.0 mmol), the mixture was stirred for 20 min, and then MeOH (100 mL) was added. After the mixture was allowed to stand overnight, 598 mg of brown-red microcrystals produced were filtered off, washed with MeOH and Et_2O in turn, and dried in a vacuum. Yield: ∼88%. Anal. Calcd for $C_{20}H_{11}ClN_5PtS_4$ (680.1): C, 35.3; H, 1.63; N, 10.3. Found: C, 35.1; H, 1.66; N, 10.2. IR spectrum (cm^{-1}): ν(CN), 2207.4 s, 2184.6 sh; ν(C═C) of mnt^{2-}, 1485.9 m.

(20) Alvarez, S.; Vicente, R.; Hoffman, R. *J. Am. Chem. Soc.* **1985**, *107*, 6253.
(21) Itkis, M. E.; Chi, X.; Cordes, A. W.; Haddon, R. C. *Science* **2002**, *296*, 1443.
(22) (a) Iwai, S.; Tanaka, S.; Fujinuma, K.; Kishida, H.; Okamoto, H.; Tokura, Y. *Phys. Rev. Lett.* **2002**, *88*, 057402. (b) Pytte, E. *Phys. Rev. B* **1974**, *10*, 4637.
(23) (a) Rettig, S. J.; Thompson, R. C.; Trotter, J.; Xia S. *Inorg. Chem.* **1999**, *38*, 1360. (b) Gao, E. Q.; Bai, S. Q.; Wang, Z. M.; Yan, C. H. *J. Am. Chem. Soc.* **2003**, *125*, 4984. (c) Tsukada, I.; Sun, X. F.; Komiya, S.; Lavrov, A. N.; Ando, Y. *Phys. Rev. B* **2003**, *67*, 224401.
(24) Bulgarevich, S. B.; Bren, D. V.; Movshovic, D. Y.; Finocchiaro P.; Failla, S. *J. Mol. Struct.* **1994**, *317*, 147.
(25) Davison A.; Holm, H. R. *Inorg. Synth.* **1967**, *10*, 8.

[BrbzPy][Pt(mnt)$_2$] (2) and [NO$_2$BzPy][Pt(mnt)$_2$] (3). The procedures for preparing **2** and **3** were similar to that for **1**. Yield of **2**: ~86%. Anal. Calcd for $C_{20}H_{11}BrN_5PtS_4$: C, 33.2; H, 1.53; N, 9.67. Found: C, 32.9; H, 1.52; N, 9.68. IR spectrum (cm^{-1}): ν(CN), 2207.9 s, 2186.5 sh; ν(C═C) of mnt^{2-}, 1485.6 m. Yield of **3**: 82%. Anal. Calcd for $C_{20}H_{11}N_6PtO_2S_4$: C, 34.8; H, 1.61; N, 12.2. Found: C, 35.0; H, 1.63; N, 12.1. IR spectrum (cm^{-1}): ν(CN), 2212.8 sh, 2208.4 s, 2183.7 sh; ν(C═C) of mnt^{2-}, 1486.8 m.

All single crystals suitable for the X-ray structure analysis were obtained by evaporating the MeCN and 1-PrOH (v/v = 1/1) mixed solution of these complexes.

Physical Measurements. Elemental analyses were performed with a Perkin-Elmer 240 analytical instrument. IR spectra with KBr pellets in the 4000−400 cm^{-1} region were obtained with an IFS66V FT-IR spectrophotometer. Magnetization measurements were carried out with a Quantum Design MPMS-7 superconducting quantum interference device (SQUID) magnetometer. DSC experiments were performed with a Perkin-Elmer calorimeter. Thermal analyses of polycrystalline samples for **1** and **2** placed in an aluminum crucible were carried out on warming (rate of 20 K min^{-1}) from −50 to +10 °C (223−283 K). The DSC experiment for **3** was performed on a PPMS model 6000 (Quantum Design) equipped with a standard Platinum 100 resistance bridge at a warming rate of 1 K min^{-1} in the temperature range of 2−300 K.

Structure Determinations. A CCD area detector (Bruker-SMART) was used for the data collection of **1** and **3** at 293 K, and a Stoe IPDS diffractometer with an imaging plate detector for **2** at 293 and 173 K. The crystallographic data and details of the data collection are given in Table 4. All computations were carried out via a PC-586 computer using the SHELXTL-PC program package.[26] The structures were solved by direct methods and refined on F^2 by full-matrix least-squares methods. All the non-hydrogen atoms were refined anisotropically. Hydrogen atoms were placed in their calculated positions and refined following the riding model.

Acknowledgment. We thank Prof. Q. P. Dai, Ms. Z. R. Yuan, and Mrs. G. Siegle for DSC analyses and Ms. E. Brücher for magnetic susceptibility measurements. This project was financially supported by the National Natural Science Foundation (Grant Nos. 29771017, 29831010, and 20171001) and the Ministry of Science and Technology (Grant No. NKBRSF-G19990646) of China. X.M.R. acknowledges financial support from the Max-Planck Society.

Supporting Information Available: EPR spectra measured at room temperature, X-ray crystallographic data for **1**−**3** at 293 K and **2** at 173 K (CIF files), powder X-ray diffraction patterns for three compounds at room temperature, and susceptibility measured under different magnetic fields. This material is available free of charge via the Internet at http://pubs.acs.org.

IC035405+

(26) Sheldrick, G. M. *SHELXTL, Structure Determination Software programs*, Version 5.10; Bruker Analytical x-ray Systems Inc.: Madison, WI, **1997**.